Journal of Sound and Vibration 329 (2010) 4109–4123

Contents lists available at ScienceDirect

Journal of Sound and Vibration

journal homepage: www.elsevier.com/locate/jsvi

# Active–passive vibration absorber of beam–cart–seesaw system with piezoelectric transducers

J. Lin *, C.J. Huang, Julian Chang, S.-W. Wang

*Department of Mechanical Engineering, Ching Yun University, 229, Chien-Hsin Road, Jung-Li City, Taiwan 320, ROC*

ARTICLE INFO

*Article history:*
Received 6 October 2009
Received in revised form
14 April 2010
Accepted 20 April 2010
Handling Editor: D.J. Wagg
Available online 15 May 2010

ABSTRACT

In contrast with fully controllable systems, a super articulated mechanical system (SAMS) is a controlled underactuated mechanical system in which the dimensions of the configuration space exceed the dimensions of the control input space. The objectives of the research are to develop a novel SAMS model which is called beam–cart–seesaw system, and renovate a novel approach for achieving a high performance active–passive piezoelectric vibration absorber for such system. The system consists of two mobile carts, which are coupled via rack and pinion mechanics to two parallel tracks mounted on pneumatic rodless cylinders. One cart carries an elastic beam, and the other cart acts as a counterbalance. One adjustable counterweight mass is also installed underneath the seesaw to serve as a passive damping mechanism to absorb impact and shock energy. The motion and control of a Bernoulli–Euler beam subjected to the modified cart/seesaw system are analyzed first. Moreover, gray relational grade is utilized to investigate the sensitivity of tuning the active proportional-integral-derivative (PID) controller to achieve desired vibration suppression performance. Consequently, it is shown that the active–passive vibration absorber can not only provide passive damping, but can also enhance the active action authority. The proposed software/hardware platform can also be profitable for the standardization of laboratory equipment, as well as for the development of entertainment tools.



## 1. Introduction

Control of underactuated systems has received considerable attention. In contrast with fully controllable systems, a super articulated mechanical system (SAMS) is a controlled underactuated mechanical system in which the dimensions of the configuration space exceed the dimensions of the control input space. For instance, an inverted pendulum on a cart, the ball and beam problem, a mass sliding on a cart, robots with joint elasticity, an underactuated bipedal robot, and nonholonomic mobile robots are all SAMSs [1,2]. Studies [3–6] of motion and control planning of nonholonomic systems have identified the difficulty yet interesting features of control synthesis for SAMSs.

The ball and beam system is a common control laboratory experiment for undergraduates [7]. The ball and beam mechanism typically comprises a ball on a beam. The ball rolls along the beam as the beam angle changes. Control of this ball and beam system has been widely investigated. However, discovering a control law that stabilizes this system remains an active area of research.

* Corresponding author. Tel.: +886 3 4581196x3760; fax: +886 3 4598411.
*E-mail address:* jlin@cyu.edu.tw (J. Lin).

0022-460X/$ - see front matter © 2010 Elsevier Ltd. All rights reserved.
doi:10.1016/j.jsv.2010.04.023

The ball and beam system has both nonlinear and unstable characteristics. Hence, several approaches, such as input–output feedback linearization [8], robust nonlinear control [9,10] and fuzzy logic control [11–13], have been developed to control the ball and beam system. However, these schemes are based on the same conventional ball-on-beam plant, in which the ball rolls along the beam in response to beam angle changes. Notably, this system lacks a mechanism for other control purposes. Furthermore, a literature review indicates that no researcher has attempted to control a ball and beam mechanism using a pneumatic cylinder for actuation. Thus, this work proposes a novel ball-and-beam-like mechanism called the cart–seesaw system [14]. The seesaw can only rotate on a vertical plane with one degree of freedom (dof), and the cart slides along the seesaw in response to a force applied by a pneumatic device. Notably, this system has only one sliding cart.

Moreover, many studies [15–20] have elucidated the dynamic responses of a flexible beam with a moving cart. Such systems occur when high-speed trains travel on railroad tracks and bridges, with overhead cranes, during high-speed precision machining and when computer disk drives are used for data storage [21]. When used in a system with flexible structures, piezoelectric materials are bonded to the body structure using a strong adhesive. A structure with an integrated distributed piezoelectric sensor and actuator was described in [22–26]. These studies demonstrated that the distributed piezoelectric sensing layer monitors structural oscillation via the converse piezoelectric effect. However, all these studies limited their focus to vibration control of a laminated beam, and no study has developed a control methodology for an elastic beam fixed onto a moving cart. This work applies a novel approach for a high-performance piezoelectric absorber in the beam–cart system in [21]. In reality, vibration of an elastic beam is markedly affected by the moving cart, particularly during reciprocal cart motion. However, this work only deals with the beam–cart system; that is, it does not address an elastic beam subjected to a seesaw mechanism.

Hence, this work extends the results of the author's previous work [14]. The motion and control of a Bernoulli–Euler beam subjected to the modified cart/seesaw system are analyzed first. Moreover, this work presents a novel active–passive vibration absorber with gray relational analysis for tuning PID control parameters of an active controller. The experimental apparatus is used to assess the efficiency of the proposed scheme. This work will serve as a reference for achievable control behavior for an underactuated mechanism, and extends existing curriculum to the control of underactuated robots. Moreover, the proposed software/hardware platform can also be profitable for the standardization of laboratory equipment, as well as for the development of entertainment tools.

## 2. System configuration

Fig. 1 schematically depicts a beam–cart–seesaw system. Fig. 2 shows this beam–cart–seesaw system and some important devices in such a system. The system consists of two mobile carts coupled via rack-and-pinion mechanics to two parallel tracks mounted on pneumatic rodless cylinders. The cylinder was double-acting. One cart carries an elastic beam,

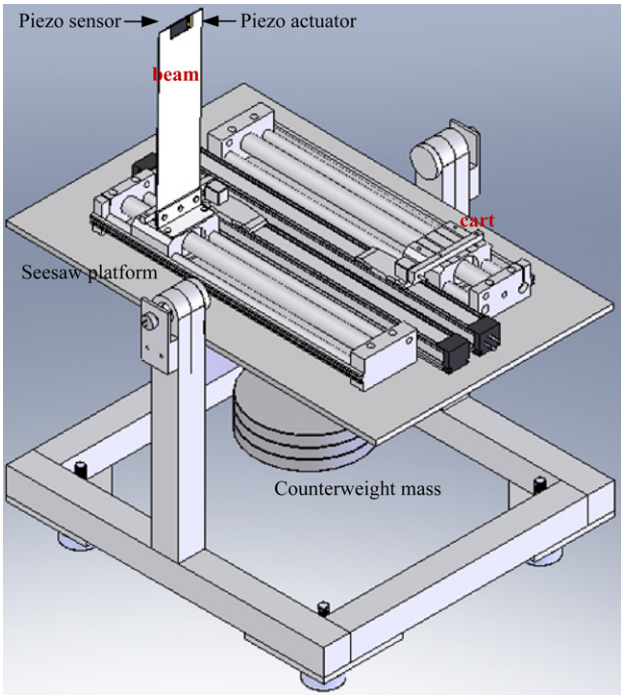


**Fig. 1.** Conceptual model of an elastic beam subjected to the cart/seesaw system.

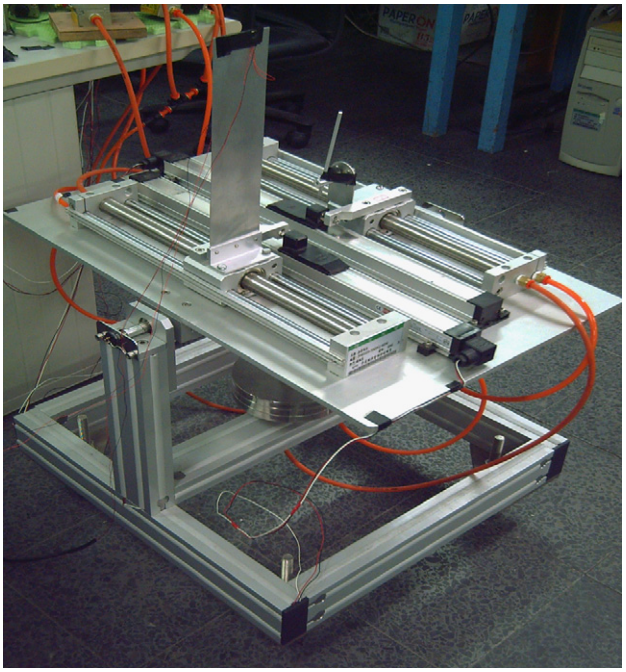

**Fig. 2.** Visualization of the beam–cart–seesaw system.

and the other cart acts as a counterbalance. Forces are applied to each cart. The seesaw was jointed and freely rotated in unison about the pivot point. A linear potentiometer was utilized to determine the position of the sliding cart, and rotary potentiometers were adopted to determine the seesaw and beam angles. Cart position was evaluated from the seesaw center, and was positive when the cart was on the right side of the seesaw. Similarly, the seesaw angle was positive when the seesaw rotated counterclockwise relative to the horizon.

Furthermore, the seesaw falls to the definite up–down direction instantaneously when the cart travels to a particular place, thereby creating instantaneous dynamic instability. Hence, as a dynamic improvement, an adjustable counterweight is installed underneath the seesaw and functions as a damping mechanism absorbing impact and shock energy. This mechanism is called as the dynamic balance apparatus.

The experimental pneumatic system comprised two pneumatic rodless cylinders, each 510 mm long, four controlled proportional valves, and a compressed air source. The air supplied to the cylinder was controlled by an electro-pneumatic transducer that provided air pressure proportional to supplied voltage. Each motion direction was selected by appropriate actuation of the $\frac{3}{2}$-way electro-valves (model type, SMC VEF 3121-1), which converted electrical signals into proportional airflow. Fig. 3 shows the pneumatic control circuit.

## 3. Dynamic modeling

This section introduces a mathematical model of the elastic beam subjected to the cart/seesaw system, as acquired from known dynamics. Fig. 4 shows the proposed beam–cart–seesaw system. The beam–cart–seesaw system brings the cart from an initial position at any initial speed to a desired position on the seesaw by applying an appropriate force to the cart and, thus, adjusting the seesaw angle. Carts 1 and 2 sliding along the seesaw have one and two dof, respectively, which are actuated by a pneumatic proportional control valve. The angle of the seesaw and elastic beam are the third and fourth dof, respectively, both of which are not actuated. Even if the beam is considered to mounted on a moving cart and it may need large surface, the wind force can be negligible in the modeling owing to little effect on assumption for the wind force on the system.

Let the moment of inertia of the seesaw be $J$, gravitational acceleration be $g$, and the mass of sliding Carts 1 and 2 be $m_1$ and $m_2$, respectively. The counterweight mass, $m_3$, with length $l_3$ is attached underneath the seesaw and serves as the vibration damper absorbing impact and shock energy. The counterweight vibration absorber only considers the counterweight mass as a damping mechanism, therefore, no damping factor need to be discussed for the counterweight mass.

The mass per unit length of the elastic beam is $\gamma$, elastic beam length is $l$, and flexural rigidity of the unloaded beam is $EI$. Additionally, $\theta$ is the seesaw angle, $\beta$ is the elastic beam angle, and $F_1$ and $F_2$ are the force applied to Carts 1 and 2, respectively. Consequently, the entire system can be divided into the following five subsystems: Cart 1; Cart 2; the

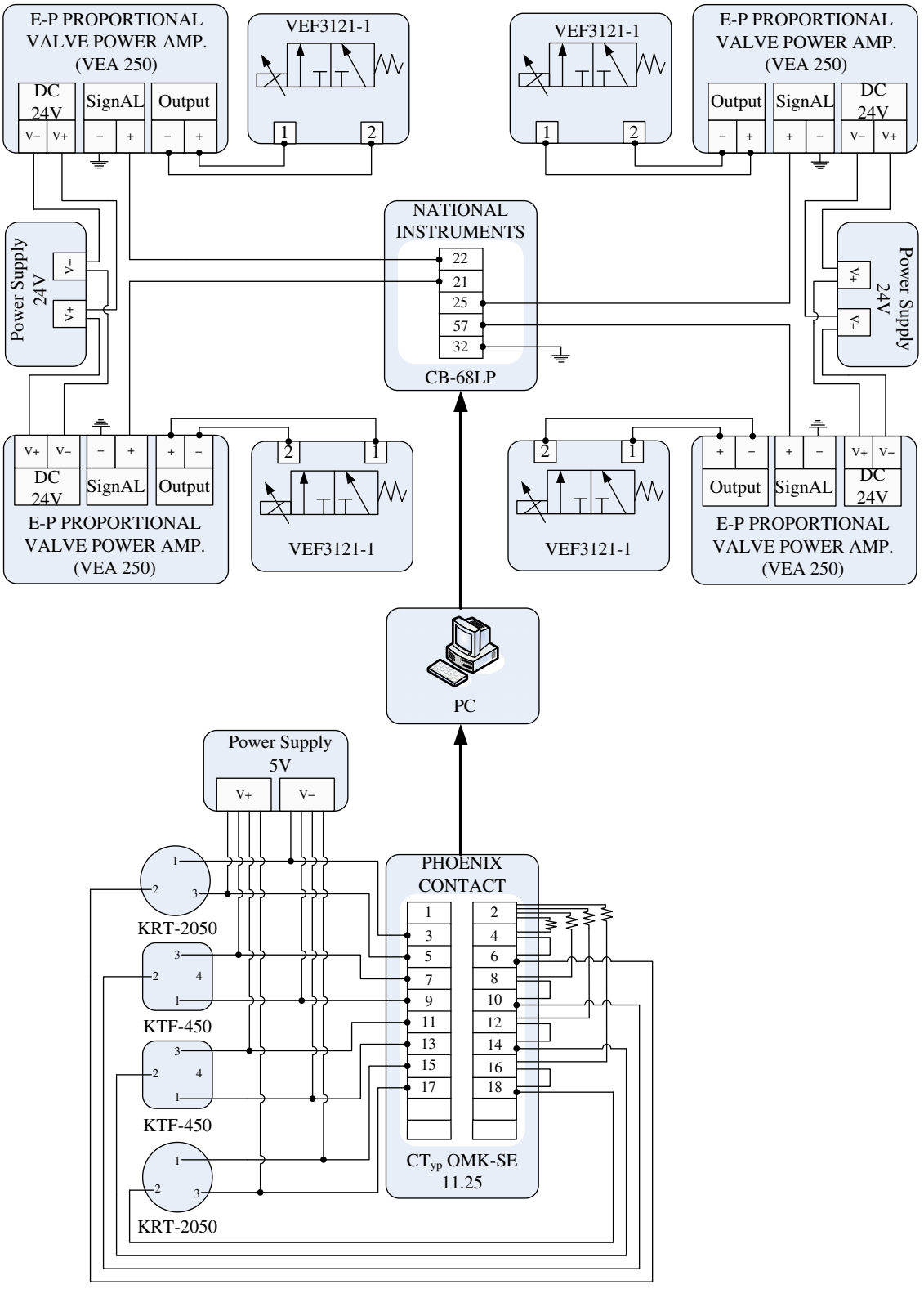


**Fig. 3.** Pneumatic control circuit.

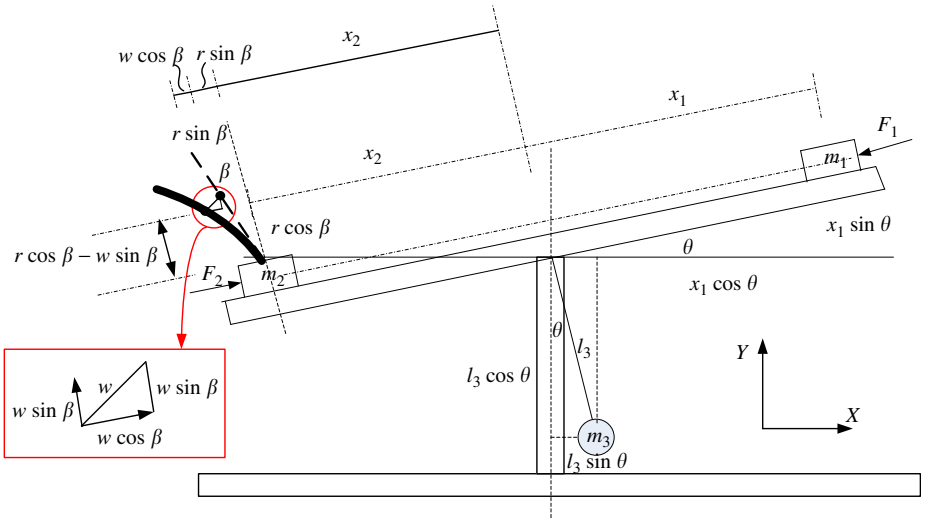


**Fig. 4.** Dynamic model for beam–cart–seesaw system.

counterweight mass; seesaw; and, elastic beam. Thus, the kinetic energy and potential energy for each subsystem can be computed and the global dynamic equations can then be derived.

Assuming a Bernoulli–Euler beam model, the deflection of an elastic beam $w(r,t)$ can be expressed as the sum of an infinite series terms

$$w(r,t) = \sum_{i=1}^{n} q_i(t)\phi_i(r) \tag{1}$$

where $q_i(t)$ are generalized modal coordinates; $\phi_i(r)$ are mode-shape functions that depend upon the boundary value problem; and $n$ is the number of retained modes [21].

Additionally, total kinetic energy, $K(t)$, and potential energy, $P(t)$, are derived as

$$K(t) = K_c(t) + \int_0^l K_b(r,t)dr \tag{2}$$

$$P(t) = P_c(t) + \int_0^l P_b(r,t)dr \tag{3}$$

where $K_c(t)$ and $P_c(t)$ are the kinetic and potential energy functions resulting from motion of the carts, seesaw, and counterweight mass; and $K_b(r,t)$ and $P_b(r,t)$ are the kinetic and potential energy density functions resulting from beam flexibility, respectively. Thus, total kinetic energy of the entire system can be written as

$$\begin{aligned} K = {} & \frac{1}{2}m_1(\dot{x}_1^2 + x_1^2\dot{\theta}^2) + \frac{1}{2}m_2(\dot{x}_2^2 + x_2^2\dot{\theta}^2) + \frac{1}{2}m_3 l_3^2\dot{\theta}^2 + \frac{1}{2}J\dot{\theta}^2 \\ & + \frac{1}{2}\gamma\int_0^l \left\{ \begin{array}{l} \dot{x}_2^2 + x_2^2\dot{\theta}^2 + r^2\dot{\beta}^2 + \left(\sum_{i=1}^{n}\phi_i\dot{q}_i\right)^2 + \dot{\beta}^2\left(\sum_{i=1}^{n}\phi_i q_i\right)^2 + 2r\dot{\beta}\left(\sum_{i=1}^{n}\phi_i\dot{q}_i\right) + r^2\dot{\theta}^2 + \dot{\theta}^2\left(\sum_{i=1}^{n}\phi_i q_i\right)^2 \\ \quad + [2\dot{x}_2 r\dot{\beta} + 2\dot{x}_2\left(\sum_{i=1}^{n}\phi_i\dot{q}_i\right) + 2x_2\dot{\theta}^2\left(\sum_{i=1}^{n}\phi_i q_i\right)]\cos\beta - [2\dot{x}_2\dot{\beta}\left(\sum_{i=1}^{n}\phi_i q_i\right) - 2x_2 r\dot{\theta}^2]\sin\beta \end{array} \right\} dr \end{aligned} \tag{4}$$

Similarly, total potential energy can be derived as

$$P = m_1 g x_1 \sin\theta + m_2 g x_2 \sin\theta - m_3 g l_3 \cos\theta + \frac{1}{2}EI\int_0^l \left[\sum_{i=1}^{n}\phi''_i(r)q_i(t)\right]^2 dr \tag{5}$$

By selecting slide carts positions $x_1$ and $x_2$, seesaw angle $\theta$, beam angle $\beta$, and flexible modal coordinates $q_i(t)$ as generalized system coordinates, and by using the Lagrangian formulation, the dynamic equations can be rewritten as

$$\mathbf{M}(\psi)\ddot{\psi} + \mathbf{N}(\psi,\dot{\psi}) + \mathbf{G}(\psi) + \mathbf{K}(\psi) = \tau \tag{6}$$

where $\psi = [x_1\ x_2\ \theta\ \alpha\ q_1\ q_2\ q_n]^T$; $\mathbf{M}$ is the inertial matrix, $\mathbf{N}$ is Coriolis/centripetal matrix, $\mathbf{G}$ is the gravity matrix, $\mathbf{K}$ is the stiffness matrix, and $\tau = \begin{bmatrix} u_1 & u_2 \end{bmatrix}^T$, where $u_1$ is the force applied to each cart driven by a voltage command from the pneumatic servo valve, $u_1 = \begin{bmatrix} F_1 & F_2 \end{bmatrix}^T$; and $u_2$ is the control voltage from the piezo-actuator.

Thus, the dynamic equation can be shown as the following matrix form:

$$\begin{bmatrix} M_{11} & 0 & 0 & 0 & 0 & 0 & \cdots & 0 \\ 0 & M_{22} & 0 & M_{24} & M_{25_1} & M_{25_2} & \cdots & M_{25_n} \\ 0 & 0 & M_{33} & 0 & 0 & 0 & \cdots & 0 \\ 0 & M_{42} & 0 & M_{44} & M_{45_1} & M_{45_2} & \cdots & M_{45_n} \\ 0 & M_{5_12} & 0 & M_{5_14} & M_{5_15_1} & 0 & \cdots & 0 \\ 0 & M_{5_22} & 0 & M_{5_24} & 0 & M_{5_25_2} & \cdots & 0 \\ \vdots & \vdots & \vdots & \vdots & \vdots & \vdots & \vdots & \vdots \\ 0 & M_{5_n2} & 0 & M_{5_n4} & 0 & 0 & \cdots & M_{5_n5_n} \end{bmatrix} \begin{bmatrix} \ddot{x}_1 \\ \ddot{x}_2 \\ \ddot{\theta} \\ \ddot{\beta} \\ \ddot{q}_1 \\ \ddot{q}_2 \\ \vdots \\ \ddot{q}_n \end{bmatrix} + \begin{bmatrix} N_1 \\ N_2 \\ N_3 \\ N_4 \\ N_{51} \\ N_{52} \\ \vdots \\ N_{5n} \end{bmatrix} + \begin{bmatrix} G_1 \\ G_2 \\ G_3 \\ G_4 \\ 0 \\ 0 \\ \vdots \\ 0 \end{bmatrix} + \begin{bmatrix} 0 \\ 0 \\ 0 \\ 0 \\ K_{51} \\ K_{52} \\ \vdots \\ K_{5n} \end{bmatrix} = \begin{bmatrix} F_1 \\ F_2 \\ 0 \\ 0 \\ 0 \\ 0 \\ \vdots \\ 0 \end{bmatrix} + \begin{bmatrix} 0 \\ 0 \\ 0 \\ 0 \\ \phi'_1(l_0) \\ \phi'_2(l_0) \\ \vdots \\ \phi'_n(l_0) \end{bmatrix} u_2 \quad (7)$$

where $l_0$ is the location of the piezo-actuator. The details of symbolic terms in Eq. (6) are provided in Appendix 1.

The inertial matrix of the overall system, $\mathbf{M}(\psi) \in \Re^{(4+n)\times(4+n)}$, in Eq. (7) is symmetrical and positive-definite. Therefore, inertial matrix $\mathbf{M}(\psi)$, which is uniformly bounded from above and below, satisfies

$$\underline{\mathbf{m}} I_{4+n} \le \mathbf{M}(\psi) \le \overline{\mathbf{m}} I_{4+n}, \quad \forall \psi \in \Re^{4+n} \quad (8)$$

where $\underline{\mathbf{m}}$ and $\overline{\mathbf{m}}$ are positive constants, and $I_{n+p} \in \Re^{(4+n)\times(4+n)}$ is the identity matrix. The resulting equations above demonstrate that the element of the dynamic equation matrix is very complex and highly nonlinear. Because manual symbolic expansion for such system is tedious, time consuming, and prone to errors, an automated derivation process is highly desirable. Therefore, a symbolic program written in MATLAB to generate the dynamic equations for such system is used in this research.

## 4. Controller design

The control objective attempts to determine input control force $u_1$, such that the deflection of the beam $w$ damps out as efficiently as possible while the positions of the sliding carts follow the desired tracking. This section introduces a two-level control scheme. The pneumatic proportional valves drive the carts to the desired position dominated by the *position tracking controller*. Moreover, a *vibration absorber* design for a structure ultimately attempts to limit structural vibrations to the desired level by appropriately driving the piezo-actuator. However, due to space limitations, this work only focuses on the vibration suppression controller.

The controller for suppressing vibratory motion can be constructed using a piezo-material. The sensors are utilized to obtain information of modal state variables, which are further processed as modal control forces. The actual control inputs are synthesized and applied to the proposed system through the piezoelectric actuators.

Although controlling flexible structures is a complex task, one can design and employ high-performance controllers that suppress structural vibrations, thereby ensuring the closed-loop stability of the controlled system. Particularly, when actuators and sensors are collocated and compatible (e.g., collocated piezoelectric transducers), a very efficient control design approach can be generated. Therefore, the control design techniques introduced in this study assume a collocated structure.

The voltage across the faces of a distributed piezoelectric sensor subjected to strain due to beam is derived by

$$\begin{aligned} V_s(t) &= -(Q_0/C)\int_{l_1}^{l_2} w''(r,t)\eta(r)dr \\ &= (Q_0/C)(w'(l_1,t) - w'(l_2,t)) \\ &= (Q_0/C)\cdot\sum_{i=1}^{l}[\phi'_i(l_1) - \phi'_i(l_2)]q_i(t) \end{aligned} \quad (9)$$

where $Q_0$ is the charge coefficient, which depends on the piezoelectric constant and geometric parameters, $C$ is the sensor capacitance, $(r,t)$ is the beam curvature, $\eta(r)$ is the spatial distribution of the sensor segment, and $l_1$ and $l_2$ are the sensor boundary coordinates. Moreover, $_i(r)$ is the slope of the mode shape function evaluated at $x$, and $q_i(t)$ is the modal coordinate corresponding to the $i$th mode [21,25,26].

Since the vibration suppression controller is independent of cart/seesaw positioning control, the individual PID controller is easy to design for each collocated actuator–sensor pair. However, the principal challenge in designing an acceptable PID controller is tuning PID controller parameters to achieve the desired performance. The approach for selecting parameters based on experimental results is typically time-consuming. However, manual tuning is not frequently applied in practice, because it is both laborious and time-consuming, particularly for processes with large time constants. Manual tuning also requires an instrument/control engineer and operator to pay close attention to the process, because the process must be operated near instability to measure ultimate gain and period [27]. Thus, an efficient method for selecting the PID control gains of a vibration absorber is required.

This remaining subsection introduces the gray relational approach for analyzing system output (vibrational displacement) sensitivity to small perturbations in PID controller parameters. Gray relational analysis is employed to

rank the importance of PID control gains. Gray relational analysis is described as follows. The computational technology resembles that which is described elsewhere [27].

*Step 1*. Estimate the comparison series $x_j$

The vibrational displacement of an elastic beam is defined by $e_b(kT)=H(kT)-H_d(kT)$, where $H_d(kT)$ is the desired vibrational displacement (always set to zero) for the elastic beam, $H(kT)$ is the sensor signal from the piezoelectric sensor, $k$ is an integer, and $T$ is the sampling period. Thus, the comparison series $x_j$ can be defined as the vibrational displacement of the elastic beam in a normalized root-mean-square (rms) formulation

$$x_j = \sqrt{\sum_{k=1}^{N} e_H^2/N} \tag{10}$$

where $N$ is the total number of samples.

*Step 2*. Calculate the reference series $x_i$,

$$x_i^*(k) = \frac{\min[x_j^{(0)}(k)]}{x_j^{(0)}(k)} \tag{11}$$

where $\min[x_j^{(0)}(k)]$ is the minimum values in a comparison series at the $k$th experimental datum.

*Step 3*. Compare the absolute differences of a given series via

$$\Delta_{ij}(k) = |x_i(k)-x_j(k)| \tag{12}$$

where $\Delta_{ij}$ is the absolute difference between series $x_i$ and $x_j$ at the $k$th experimental datum. Typically, $x_i$ and $x_j$ are defined as reference and comparison series, respectively. The values for the original series must be normalized to the same order as variations in the order of data that characterize factors that result in an inaccurate gray relational grade (GRG).

*Step 4*. Estimate the minimum and maximum values of each experimental datum via

$$\begin{aligned} \Delta\min &= \overset{\min}{\forall j} \in \overset{\min}{i}\forall k|x_i(k)-x_j(k)| \\ \Delta\max &= \overset{\max}{\forall j} \in \overset{\max}{i}\forall k|x_i(k)-x_j(k)| \end{aligned} \tag{13}$$

*Step 5*. Estimate the gray relational coefficient (GRC) using $\gamma(x_i(k),x_j(k))$

The calculated GRC expresses the relationship between control performance, which is an estimated reference sequence, and its sequences that are compared. Eq. (14) yields the GRC of $(x_i, x_j)$ at the $k$th corresponding datum. The GRC can be intuitively considered the point-to-point relationship at the $k$th corresponding datum.

$$\gamma(x_i(k),x_j(k)) = \frac{\Delta min+\mu\Delta max}{\Delta_{ij}(k)+\mu\Delta\max} \tag{14}$$

where $\mu$ is the distinguishing coefficient; its interval is bounded on $\mu\in[0,1]$ and frequently taken as 0.5. The factor $\mu$ in Eq. (14) controls the resolution between $\Delta$max and $\Delta$min. The operator can select a value between 0 and 1 that is best suited to the application. Additionally, $\Delta$min and $\Delta$max are the minimum and maximum differences between the reference sequence and all other sequences, respectively.

*Step 6*. Estimate the gray relationship grade (GRG) $\Pi(x_i,x_j)$

The GRG is employed to describe and elucidate the relationship between two sets of comparisons and references under a particular background. A large GRG between two tasks indicates that the tasks are closely related. In other words, tasks that are very similar have a large GRG. When estimating the effort expended by a PID controller, the GRG is the strength of the relationship between an estimated control performance (reference series) and its historical values (comparison series). The GRG is defined as the mean of GRCs of the effort drivers. Here, $\Pi(x_i,x_j)$ is designed as the GRG between $x_i(k)$ and $x_i(k)$

$$\Pi(x_i,x_j) = \frac{1}{m}\sum_{k=1}^{m}\gamma(x_i(k),x_j(k)) \tag{15}$$

where $m$ is the number of effort drivers identified during the estimation procedure. In the vibration suppression control experiment, the GRG is associated with the impact of the PID control gains for vibration damping.

## 5. Results and discussion

An experimental apparatus was constructed and presented (Fig. 5). The beam–cart–seesaw system consists of two mobile carts, which are coupled via rack and pinion mechanics to two parallel tracks mounted on pneumatic rodless cylinders. One cart carries an elastic beam, while the other one serves as a counterbalance. Four solenoid proportional direction control valves were used to drive the two double-acting pneumatic rodless cylinders. The air supply was controlled at 6 bar (6 kg f/cm$^2$). The controller of the beam–cart–seesaw system is composed of two National Instruments

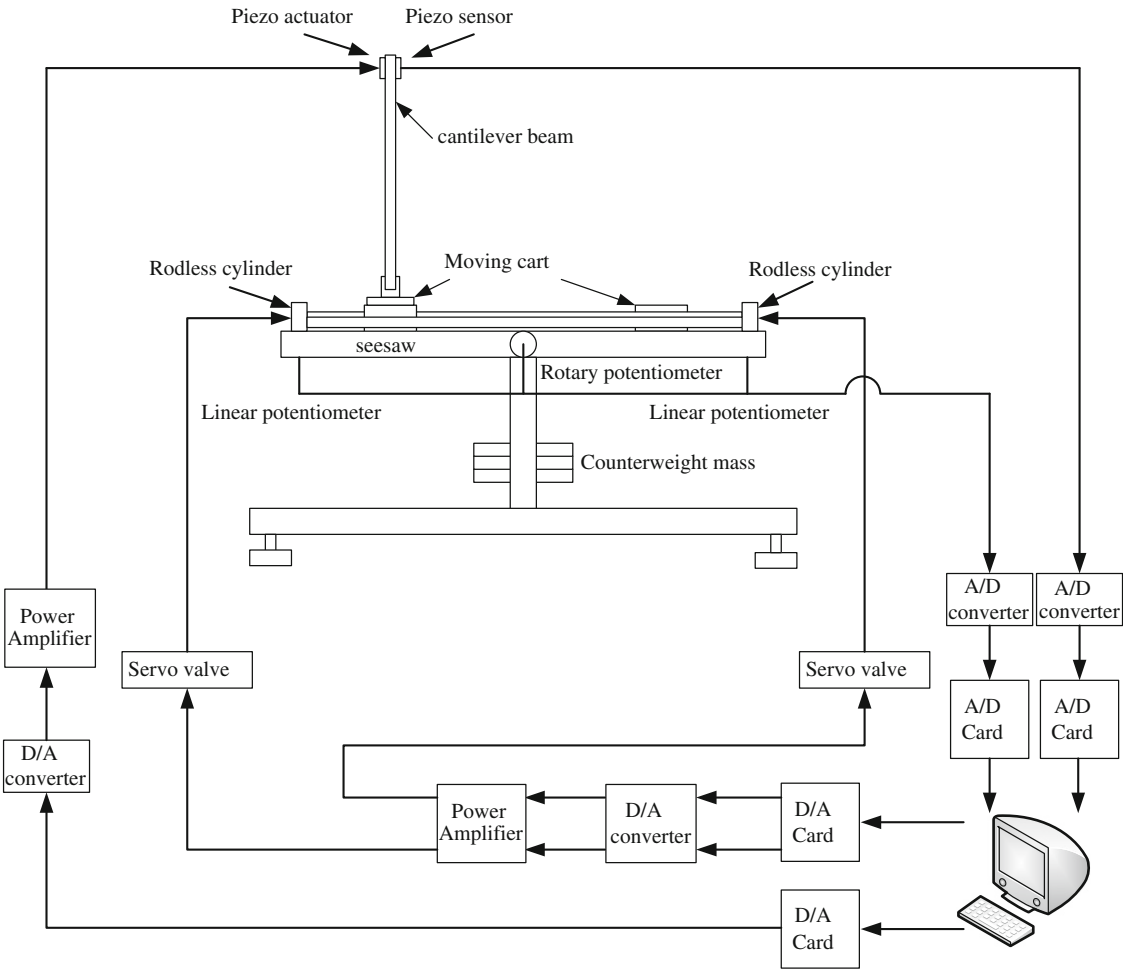


**Fig. 5.** Controller implementation.

(NIs) Data Acquisition (DAQ) boards (the PCI-MIO-16E-4 and PCI-6174) and a host personal computer. The real-time software interface of the controller board permits rapid control prototyping using LabVIEW, thereby enabling a quick implementation of the proposed control approach using the real-time block model applied in LabVIEW. Furthermore, a flexible cantilever aluminum-beam-type structure with piezoelectric patches was symmetrically bonded on both sides to permit structural bending. The cantilever beam was clamped at one end and free at the other end. Strip-bender-type 401010 (made by American Piezo Ceramics, Inc.) piezoelectric patches were attached to the beam surfaces and acted as actuators (where input signals are applied) and a sensor (where output signals are recorded). The voltage from the piezoelectric sensor was utilized to evaluate the beam vibration level. Hence, the control work attempts to suppress vibrations of this beam–cart–seesaw system using a PID vibration suppression control structure. The feedback voltage applied across the piezoelectric actuator can be determined using the control algorithm in Section 4.

Gray relational analysis is performed to determine the sensitivity of PID vibration controller parameters and achieve the desired damping performance. Calculation of the GRG follows the steps outlined in Section 4. Table 1 presents the computational results yielded by Eqs. (10)–(15) for vibration suppression of an elastic beam. Table 1 presents the normalized rms tracking error, $e_b$, for various $k_{bp}$, $k_{bi}$, and $k_{bd}$ control gains. Table 1 also shows the GRC $\gamma$ and its relational grade, $\Pi$. The GRG $\Pi$ is 0.94082 for $k_{bp}$, 0.91509 for $k_{bd}$, and 0.90899 for $k_{bi}$. Hence, the sensitivities of parameter perturbations are obtained easily. Furthermore, the PID vibration controller is more sensitive for tuning $k_{bp}$ than for tuning $k_{bd}$ and $k_{bi}$ (Table 1). The ranked importance of control gains is $k_{bp} > k_{bd} > k_{bi}$. The most important parameter typically dominates during base control; the next most important parameters are used to modify fine motion. Hence, control parameters with the highest priorities should be modified first. Based on the GRG between tracking error and PID control gains, all control gains can be ranked according to their GRGs—this procedure is called gray relational ranking. Consequently, an operator can make an appropriate decision based on the gray ranking and the control goal can be achieved. Fig. 6 shows the modification process.

**Table 1**
Grey relational grade for the vibration suppression controller of an elastic beam.

| Design | | | Eq. (10) $x_j$ | Eq. (11) $x_i$ | Eq. (12) $\Delta_{ij}$ | Eq. (14) $\gamma(x_j(k), x_i(k))$ | Eq. (15) $\Pi(x_j, x_i)$ | Rank |
|---|---|---|---|---|---|---|---|---|
| $k_{bp}$=500 | $k_{bp}$=500 | $k_{bi}$=0 | 0.04886 | 0.87778 | 0.82892 | 0.96672 | **0.94082** | 1 |
| $k_{bp}$=600 | | | 0.04289 | 1.00000 | 0.95710 | 0.88044 | | |
| $k_{bp}$=700 | | | 0.04532 | 0.94646 | 0.90114 | 0.91614 | | |
| $k_{bp}$=800 | | | 0.05126 | 0.83665 | 0.78538 | 1.00000 | | |
| $k_{bp}$=600 | $k_{bp}$=500 | $k_{bi}$=0 | 0.04289 | 1.00000 | 0.95710 | 0.88044 | **0.91509** | 2 |
| | $k_{bp}$=600 | | 0.04462 | 0.96124 | 0.91661 | 0.90598 | | |
| | $k_{bp}$=700 | | 0.04598 | 0.93277 | 0.88678 | 0.92577 | | |
| | $k_{bp}$=800 | | 0.04755 | 0.90205 | 0.85450 | 0.94817 | | |
| $k_{bp}$=600 | $k_{bp}$=500 | $k_{bi}$=0.5 | 0.04588 | 0.90602 | 0.86013 | 0.94419 | **0.90899** | 3 |
| | | $k_{bi}$=1 | 0.04157 | 1.00000 | 0.95842 | 0.87963 | | |
| | | $k_{bi}$=1.5 | 0.04321 | 0.96197 | 0.91875 | 0.90459 | | |
| | | $k_{bi}$=2 | 0.04341 | 0.95760 | 0.91419 | 0.90756 | | |
| | | | | | ↓ | | | |
| | | | | Eq. (13) | | | | |
| | | | | $\Delta_{min}$ | $\Delta_{max}$ | | | |
| | | | | 0.78538 | 0.95842 | | | |

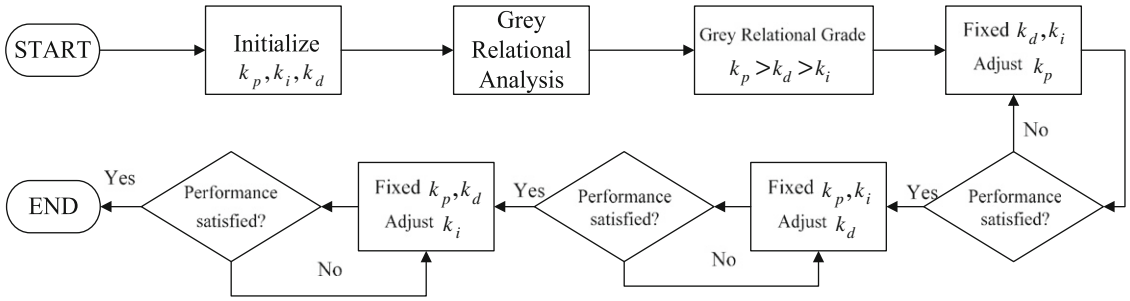


**Fig. 6.** Flowchart of the parameter modification process.

### 5.1. *Experimental results of vibration suppression at the equilibrium point of the seesaw*

As mentioned in Section 4, vibration control must only select control gains for vibration suppression. Thus, redesigning a vibration-damping controller for such a system is unnecessary. Therefore, to further confirm controller performance, vibration suppression around the seesaw equilibrium point was applied to the system. The seesaw falls toward the definite direction instantaneously when the cart moves to a particular location, thus creating instantaneous dynamic stability without a counterweight mass. Therefore, to investigate counterweight mass damping capability (passive control), various counterweight mass lengths are discussed.

#### 5.1.1. *Case 1: carts sliding with a small displacement around the equilibrium point*

First, this work investigates carts sliding with a small displacement around the equilibrium point. Fig. 7 plots the time response for carts position (Fig. 7(a)) and seesaw angle (Fig. 7(b)) of Case 1. Both carts start at the seesaw midpoint and try to keep the seesaw in the equilibrium state. One cart carries an elastic beam and the other cart functions as a counterbalance. Table 2 lists the normalized rms piezo-sensor output voltage under uncontrolled, passive, active–passive absorber for various counterweight mass lengths $l_3$. It is worth noting that if the counterweight mass $l_3$=0, it means that the counterweight mass tightly attaches to the seesaw platform. The counterweight mass has a damping capability that stabilizes the dynamic system. Moreover, the vibratory displacement decreases in magnitude while the counterweight mass device far from the seesaw (Table 2). Consequently, the proposed counterweight mass device markedly improved the performance of seesaw equilibrium motion and vibration suppression for an elastic beam. The counterweight mass device can serve as a damping mechanism that absorbs impact, shock, and vibration energy. Although economical, passive control can only control vibrations up to a certain limit. Conversely, an active control operates with external energy supplied continuously. Namely, this work is applied an active piezoelectric absorber to an elastic beam.

According to the gray relational degree described in Section 4, parameter $k_{bp}$ is first adjusted to yield the best vibration suppression for an elastic beam. Parameters $k_{bd}$ and $k_{bi}$ are then adjusted to acquire the best performance for reference inputs for the remaining operational range. After arbitrarily assigning values to PID parameters ($k_{bp}$=600, $k_{bi}$=1, and $k_{bd}$=500), the modification process is applied (Fig. 6). First, the adjusted sequence for control parameters for vibration

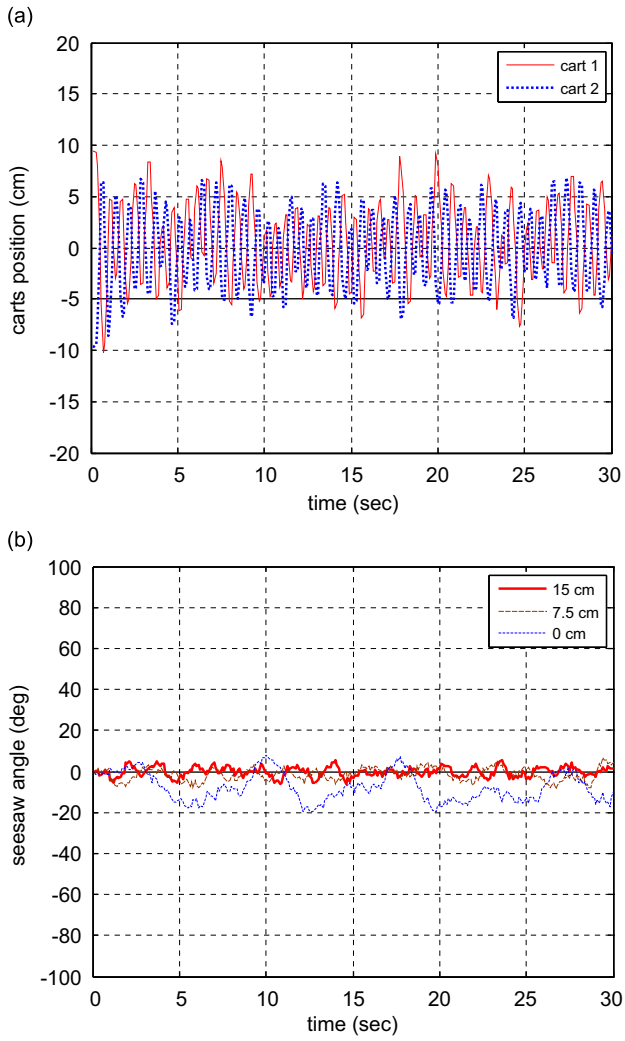


**Fig. 7.** Time response for (a) carts position and (b) seesaw angle (Case 1).

**Table 2**
Normalized RMS vibrational displacements of a beam (Case 1).

| Uncontrolled (A) | Passive control (B) | Active–passive absorber (C) | | Reduction $[(A-C)/A]\times 100\%$ (%) | Reduction $[(B-C)/B]\times 100\%$ (%) |
|---|---|---|---|---|---|
| 0.135094 | $l_3$=15 cm | $k_{bp}$=600, $k_{bi}$=1, $k_{bp}$=500 | 0.04157 | 69.22 | 0.512 |
| | 0.04178 | $k_{bp}$=610, $k_{bi}$=1, $k_{bd}$=500 | 0.03854 | 71.47 | 7.76 |
| | | $k_{bp}$=610, $k_{bi}$=1, $k_{bd}$=460 | 0.03711 | 72.53 | 11.19 |
| | | $k_{bp}$=610, $k_{bi}$=1.1, $k_{bd}$=460 | 0.03510 | 74.01 | 15.59 |
| | $l_3$=7.5 cm | $k_{bp}$=620, $k_{bi}$=1.1, $k_{bd}$=460 | 0.03972 | 70.59 | 13.54 |
| | 0.04594 | $k_{bp}$=630, $k_{bi}$=1.1, $k_{bd}$=460 | 0.03857 | 71.44 | 16.04 |
| | | $k_{bp}$=630, $k_{bi}$=1.1, $k_{bd}$=490 | 0.03677 | 72.78 | 19.95 |
| | | $k_{bp}$=620, $k_{bi}$=1.2, $k_{bd}$=490 | 0.03472 | 74.30 | 24.42 |
| | $l_3$=0 cm | $k_{bp}$=640, $k_{bi}$=1.2, $k_{bd}$=490 | 0.04339 | 67.88 | 15.62 |
| | 0.05143 | $k_{bp}$=650, $k_{bi}$=1.2, $k_{bd}$=490 | 0.03909 | 71.06 | 23.99 |
| | | $k_{bp}$=650, $k_{bi}$=1.2, $k_{bd}$=500 | 0.03627 | 73.15 | 29.47 |
| | | $k_{bp}$=650, $k_{bi}$=1.3, $k_{bd}$=500 | 0.03575 | 73.53 | 30.48 |

suppression is

$$(k_{bp}=600,\ k_{bi}=1,\ k_{bd}=500)\rightarrow(k_{bp}=610,\ k_{bi}=1,\ k_{bd}=500)$$
$$\rightarrow(k_{bp}=610,\ k_{bi}=1,\ k_{bd}=460)\rightarrow(k_{bp}=610,\ k_{bi}=1.1,\ k_{bd}=460)$$

Performance improved significantly after this modification methodology was applied to the control parameters (Table 2). Suppression performance was improved significantly by tuning control parameter $k_{bp}$. The vibrational displacement response was decreased markedly by the control action, indicating that parameter $k_{bp}$ in the controller is the most important parameter and dominates base control action. However, the enhanced performance achieved by tuning only parameter $k_{bp}$ is insignificant and vibrational displacement remains large. Therefore, tuning $k_{bd}$ and then $k_{bi}$ significantly improves system vibration suppression. Consequently, the proposed modification scheme reduces vibrational displacement. The performance of the active–passive absorber is markedly better than that of passive damping for vibration reduction. The proposed active–passive absorber reduces displacement due to vibration of an uncontrolled by roughly 68–73% (Table 2). Furthermore, compared with passive control, vibrational displacement is further reduced to 0.512–30.48% by the proposed active–passive piezoelectric absorber. Evidently, a vibration reduction (%) by the active–passive absorber heavily depends on PID control values. The normalized rms is around 0.0351–0.04339 with the active–passive absorber. Such a controller suppresses the transverse deflection of the structure. Moreover, active–passive absorber performance is relatively unaffected by changes in counterweight mass length $l_3$. The proposed approach ensures that active and passive elements are configured in a systematic and integrated manner.

### 5.1.2. *Case 2: carts sliding with reciprocal motion*

Fig. 8 plots the time response for carts position (Fig. 8(a)) and seesaw angle (Fig. 8(b)) of Case 2. In this case, one cart carries an elastic beam sliding from the end of the seesaw to the other end of the seesaw. Thus, the other cart functions as a

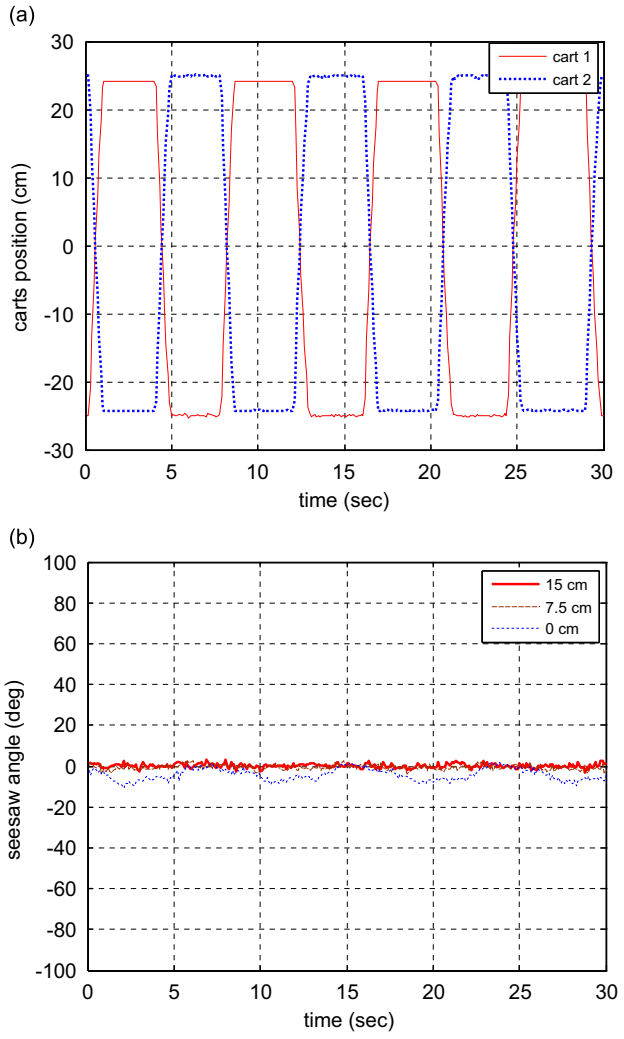


**Fig. 8.** Time response for (a) carts position and (b) seesaw angle (Case 2).

counterbalance. Therefore, the seesaw angle should always be close to zero to keep the seesaw in the equilibrium state while the carts slide. The proposed active–passive absorber reduces displacement due to vibration resulting from passive damping by approximately 7.24–30.48% for each suitable PID parameter (Table 3). Once again, the performance of

**Table 3**
Normalized RMS vibrational displacements of a beam (Case 2).

| Uncontrolled (A) | Passive control (B) | Active–passive absorber (C) | | Reduction $[(A-C)/A]\times 100\%$ (%) | Reduction $[(B-C)/B]\times 100\%$ (%) |
|---|---|---|---|---|---|
| 0.12931 | $l_3$=15 cm | $k_{bp}$=600, $k_{bi}$=1, $k_{bd}$=500 | 0.04663 | 63.93 | 7.24 |
| | 0.05026 | $k_{bp}$=620, $k_{bi}$=1, $k_{bd}$=500 | 0.04417 | 65.84 | 12.24 |
| | | $k_{bp}$=620, $k_{bi}$=1, $k_{bd}$=530 | 0.04335 | 66.41 | 13.76 |
| | | $k_{bp}$=620, $k_{bi}$=1.3, $k_{bd}$=530 | 0.04258 | 67.07 | 15.3 |
| | $l_3$=7.5 cm | $k_{bp}$=620, $k_{bi}$=1.3, $k_{bd}$=530 | 0.04987 | 61.43 | 3.25 |
| | 0.05155 | $k_{bp}$=640, $k_{bi}$=1.3, $k_{bd}$=530 | 0.04605 | 64.38 | 10.67 |
| | | $k_{bp}$=640, $k_{bi}$=1.3, $k_{bd}$=550 | 0.04460 | 65.50 | 13.49 |
| | | $k_{bp}$=640, $k_{bi}$=1.4, $k_{bd}$=550 | 0.04276 | 66.93 | 17.05 |
| | $l_3$=0 cm | $k_{bp}$=640, $k_{bi}$=1.4, $k_{bd}$=550 | 0.04540 | 64.89 | 11.71 |
| | 0.05142 | $k_{bp}$=650, $k_{bi}$=1.4, $k_{bd}$=550 | 0.04487 | 65.30 | 12.75 |
| | | $k_{bp}$=650, $k_{bi}$=1.4, $k_{bd}$=570 | 0.04275 | 66.94 | 16.87 |
| | | $k_{bp}$=650, $k_{bi}$=1.4, $k_{bd}$=570 | 0.04193 | 67.57 | 30.48 |

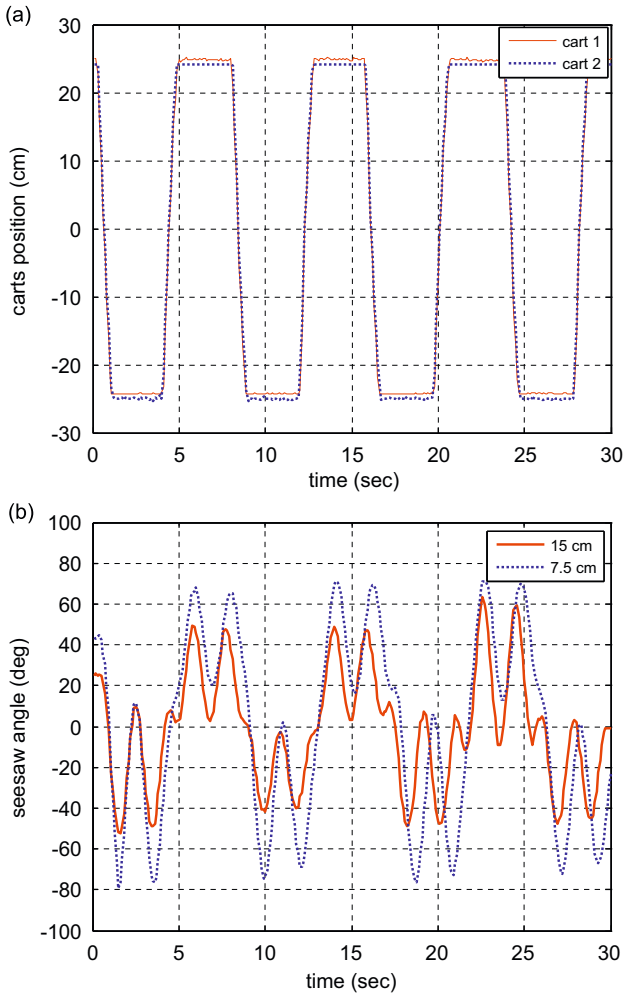


**Fig. 9.** Time response for (a) carts position and (b) seesaw angle (Case 3).

**Table 4**
Normalized RMS vibrational displacements for seesaw tilting motion.

| Uncontrolled (A) | Passive control (B) | Active–passive absorber (C) | | Reduction $[(A-C)/A]\times 100\%$ (%) | Reduction $[(B-C)/B]\times 100\%$ (%) |
|---|---|---|---|---|---|
| 0.20132 | $l_3$=15 cm | $k_{bp}$=600, $k_{bi}$=1, $k_{bd}$=500 | 0.06411 | 68.15 | 3.29 |
| | 0.06629 | $k_{bp}$=630, $k_{bi}$=1, $k_{bd}$=500 | 0.06142 | 69.49 | 7.35 |
| | | $k_{bp}$=630, $k_{bi}$=1, $k_{bd}$=520 | 0.05988 | 70.25 | 9.67 |
| | | $k_{bp}$=630, $k_{bi}$=1.3, $k_{bd}$=520 | 0.05789 | 71.24 | 12.67 |
| | $l_3$=7.5 cm | $k_{bp}$=630, $k_{bi}$=1.3, $k_{bd}$=520 | 0.07634 | 62.08 | 1.99 |
| | 0.07790 | $k_{bp}$=660, $k_{bi}$=1.3, $k_{bd}$=520 | 0.06117 | 69.61 | 21.47 |
| | | $k_{bp}$=660, $k_{bi}$=1.3, $k_{bd}$=540 | 0.05723 | 71.57 | 26.53 |
| | | $k_{bp}$=660, $k_{bi}$=1.5, $k_{bd}$=540 | 0.05574 | 72.31 | 28.44 |

the active–passive piezoelectric absorber is relatively unaffected by any change in counterweight mass length $l_3$. Hence, experimental results support the same conclusion as that for vibration suppression in Case 1.

### 5.2. Experimental results of vibration suppression for seesaw tilting motion

#### 5.2.1. Case 3: both carts slide in the same direction simultaneously

Fig. 9 plots the time response for carts position (Fig. 9(a)) and seesaw angle (Fig. 9(b)) of Case 3. In this case, both carts slide in the same direction simultaneously. Thus, the overall beam–cart–seesaw system was tilted while the carts slide. The normalized rms piezo-sensor output voltage was around 0.06629–0.00790 when implementing counterweight mass passive damping (Table 4). The proposed active–passive piezoelectric absorber reduced displacement due to vibration of a passive absorber by roughly 3.29–28.44% when the gray modification scheme was applied (Table 4). The performance of the proposed active–passive piezoelectric absorber was not significantly affected by modifying the passive absorber parameters, thereby demonstrating the effectiveness of the controller in minimizing vibrational displacement in the time domain, even when overall tilting occurs.

Hence, this study developed a novel fast adaptation scheme that used the GRG to select PID vibration control parameters for the beam–cart–seesaw system. Relational analysis was applied to easily rank the importance of PID control gains. The most important parameters were identified to ensure parameter sensitivity. The proposed gray relational methodology allows operators to adjust easily control gains during system operation.

## 6. Conclusions

This work, an extension of our previous work [14], generates a novel SAMS model called the beam–cart–seesaw system. The dynamic formulation is first proposed for control of this new elastic beam–cart–seesaw model. Moreover, the GRG is utilized to investigate the sensitivity in tuning the active PID controller to achieve the desired vibration suppression performance. The active–passive piezoelectric absorber provides passive damping, and enhances the active action authority. However, development of the proposed software/hardware platform can be profitable for standardizing laboratory equipment, and the development of entertainment tools. The proposed platform can be used with the experimental apparatus to explore the performance of such a system.

## Acknowledgements

The authors would like to thank the National Science Council of the Republic of China, Taiwan for financially supporting this research under Contract no. NSC 96-2221-E-231-017-MY3.

## Appendix 1

$$M_{11}=m_1$$

$$M_{22}=m_2+\gamma l$$

$$M_{33}=m_1x_1^2+m_2x_2^2+m_3l_3^2+J+\gamma x_2^2 l+\frac{1}{3}\gamma l^3+\gamma\left(\int_0^l\phi_1^2q_1^2+\int_0^l\phi_2^2q_2^2+\ldots+\int_0^l\phi_n^2q_n^2\right)$$
$$+2\gamma x_2\cos\beta\left(\int_0^l\phi_1q_1+\int_0^l\phi_2q_2+\ldots+\int_0^l\phi_nq_n\right)$$

$$M_{44}=\frac{1}{3}\gamma l^3+\gamma\left(\int_0^l\phi_1^2q_1^2+\int_0^l\phi_2^2q_2^2+\ldots+\int_0^l\phi_n^2q_n^2\right)$$

$$M_{5_15_1}=\gamma\int_0^l\phi_1^2;\quad M_{5_25_2}=\gamma\int_0^l\phi_2^2;\ \ldots;\quad M_{5_n5_n}=\gamma\int_0^l\phi_n^2$$

$$M_{24}=\frac{1}{2}\gamma l^2\cos\beta-\gamma\sin\beta\left(\int_0^l\phi_1q_1+\int_0^l\phi_2q_2+\ldots+\int_0^l\phi_nq_n\right)=M_{42}$$

$$M_{25_1}=\gamma\cos\beta\int_0^l\phi_1=M_{5_12};\quad M_{25_2}=\gamma\cos\beta\int_0^l\phi_2=M_{5_22};\ldots;M_{25_n}=\gamma\cos\beta\int_0^l\phi_n=M_{5_n2}$$

$$M_{45_1}=\frac{1}{2}\gamma l^2\int_0^l\phi_1=M_{5_14};\quad M_{45_2}=\frac{1}{2}\gamma l^2\int_0^l\phi_2=M_{5_24};\ \ldots;M_{45_n}=\frac{1}{2}\gamma l^2\int_0^l\phi_n=M_{5_n4}$$

$$N_1=-m_1x_1\dot\theta^2$$

$$N_2=-\frac{1}{2}\gamma\dot\beta^2l^2\sin\beta+-\gamma\dot\beta\sin\beta\left(\int_0^l\phi_1\dot q_1+\int_0^l\phi_2\dot q_2+\cdots+\int_0^l\phi_n\dot q_n\right)$$

$$-\gamma\dot\beta^2\cos\beta\left(\int_0^l\phi_1q_1+\int_0^l\phi_2q_2+\cdots+\int_0^l\phi_nq_n\right)$$

$$-\gamma\dot\beta\sin\beta\left(\int_0^l\phi_1\dot q_1+\int_0^l\phi_2\dot q_2+\cdots+\int_0^l\phi_n\dot q_n\right)$$

$$-m_2x_2\dot\theta^2-\gamma x_2\dot\theta^2l-\gamma\dot\theta^2\ s\beta\left(\int_0^l\phi_1q_1+\int_0^l\phi_2q_2+\cdots+\int_0^l\phi_nq_n\right)-\frac{1}{2}\gamma\dot\theta^2l^2\sin\beta$$

$$N_3=\gamma\dot x_2^2\dot\theta l+\gamma\dot\theta\left(\int_0^l\phi_1^2\dot q_1^2+\int_0^l\phi_2^2\dot q_2^2+\cdots+\int_0^l\phi_n^2\dot q_n^2\right)+2\gamma\dot x_2\dot\theta\cos\beta\left(\int_0^l\phi_1q_1+\int_0^l\phi_2q_2+\cdots+\int_0^l\phi_nq_n\right)$$

$$-2\gamma x_2\dot\theta\dot\beta\sin\beta\left(\int_0^l\phi_1q_1+\int_0^l\phi_2q_2+\cdots+\int_0^l\phi_nq_n\right)+2\gamma x_2\dot\theta\cos\beta\left(\int_0^l\phi_1\dot q_1+\int_0^l\phi_2\dot q_2+\cdots+\int_0^l\phi_n\dot q_n\right)$$

$$+\gamma\dot x_2\dot\theta l^2\sin\beta+\gamma x_2\dot\theta l^2\dot\beta\cos\beta$$

$$N_4=\gamma\dot\beta\left(\int_0^l\phi_1^2\dot q_1^2+\int_0^l\phi_2^2\dot q_2^2+\cdots+\int_0^l\phi_n^2\dot q_n^2\right)-\frac{1}{2}\gamma\dot x_2l^2\dot\beta\sin\beta-\gamma\dot x_2\dot\beta\cos\beta\left(\int_0^l\phi_1q_1+\int_0^l\phi_2q_2+\cdots+\int_0^l\phi_nq_n\right)$$

$$-\gamma\dot x_2\sin\beta\left(\int_0^l\phi_1\dot q_1+\int_0^l\phi_2\dot q_2+\cdots+\int_0^l\phi_n\dot q_n\right)+\frac{1}{2}\gamma\dot x_2\dot\beta l^2\sin\beta$$

$$+\gamma\dot x_2\sin\beta\left(\int_0^l\phi_1\dot q_1+\int_0^l\phi_2\dot q_2+\cdots+\int_0^l\phi_n\dot q_n\right)+\gamma x_2\dot\theta^2\sin\beta\left(\int_0^l\phi_1q_1+\int_0^l\phi_2q_2+\cdots+\int_0^l\phi_nq_n\right)$$

$$+\gamma\dot x_2\dot\beta\cos\beta\left(\int_0^l\phi_1q_1+\int_0^l\phi_2q_2+\cdots+\int_0^l\phi_nq_n\right)-\frac{1}{2}\gamma x_2\dot\theta^2l^2\cos\beta$$

$$N_{5_1}=-\gamma\dot x_2\dot\beta\sin\beta\int_0^l\phi_1-\gamma\dot\beta^2\int_0^l\phi_1^2q_1-\gamma\dot\theta^2\int_0^l\phi_1^2q_1-\gamma x_2\dot\theta^2\cos\beta\int_0^l\phi_1+\gamma\dot x_2\dot\beta\sin\beta\int_0^l\phi_1$$

$$N_{5_2}=-\gamma\dot x_2\dot\beta\sin\beta\int_0^l\phi_2-\gamma\dot\beta^2\int_0^l\phi_2^2q_2-\gamma\dot\theta^2\int_0^l\phi_2^2q_2-\gamma x_2\dot\theta^2\cos\beta\int_0^l\phi_2+\gamma\dot x_2\dot\beta\sin\beta\int_0^l\phi_2$$

$$\vdots$$

$$N_{5_n}=-\gamma\dot x_2\dot\beta\sin\beta\int_0^l\phi_n-\gamma\dot\beta^2\int_0^l\phi_n^2q_n-\gamma\dot\theta^2\int_0^l\phi_n^2q_n-\gamma x_2\dot\theta^2\cos\beta\int_0^l\phi_n+\gamma\dot x_2\dot\beta\sin\beta\int_0^l\phi_n$$

$$G_1=m_1g\sin\theta$$

$$G_2=m_2g\sin\theta$$

$$G_3=m_1gx_1\cos\theta+m_2gx_2\cos\theta+m_3gl_3\sin\theta$$

$$G_4=0$$

$$K_{5_1}=EI\int_0^l\phi''_1{}^2q_1$$

$$K_{5_2}=EI\int_0^l\phi''_2{}^2q_2$$

$$\vdots$$

$$K_{5_n}=EI\int_0^l\phi''_n{}^2q_n$$

## References


[1] S. Uran, K. Jezernik, Control of a ball and beam like mechanism, *Proceedings of the 7th International Workshop on Advanced Motion Control,* Maribor, Slovenia, 2002, pp. 376–380.
[2] G. Wang, Y. Tian, W. Hong, Stabilization and equilibrium control of super articulated ball and beam system, *Proceedings of the 3rd World Congress on Intelligent Control and Automation*, Hefei, China, 2000, pp. 3290–3293.
[3] S. Seto, J. Baillieul, Control problems in super-articulated mechanical systems, *IEEE Transactions on Automatic Control* 39 (12) (1994) 2442–2453.
[4] A.M. Bloch, M. Reyhanoglu, N.H. McClamroch, Control and stabilization of nonholonomic dynamic systems, *IEEE Transactions on Automatic Control* 39 (12) (1992) 1746–1757.
[5] G. Lafferriere, H. J. Sussmann, Motion planning for controllable systems without drift, *Proc. IEEE International Conference On Robotics and Automation,* Sacramento, California, USA, 1991, pp. 1148–1153.
[6] R.M. Murray, S.S. Sastry, Nonholonomic motion planning: steering using sinusoids, *IEEE Transactions on Automatic Control* 38 (5) (1993) 700–716.
[7] M. T. Hagan, C. D. Latino, An interdisciplinary control systems laboratory, *Proceedings of the IEEE International Conference on Control Applications*, Dearborn, MI, USA, 1996, pp. 403–408.
[8] J. Hauser, S. Sastry, P. Kokotovic, Nonlinear control via approximate input–output linearization: the ball and beam example, *IEEE Transactions on Automatic Control* 37 (3) (1992) 392–398.
[9] J. Huang, C.-F. Lin, Robust nonlinear control of the ball and beam system, *Proceedings of the American Control Conference*, Seattle, Washington, USA, 1995, pp. 306–310.
[10] A. T. Simmons, J.-Y. Hung, Hybrid control of system with poorly defined relative degree: the ball-on-beam example, *Proceedings of the 30th Annual Conference of the IEEE Industrial Electronics Society*, Busan, Korea, 2004, pp. 2436–2440.
[11] H. K. Lam, F. H. F. Leung, P. K. S. Tam, Design of a fuzzy controller for stabilizing a Ball-and-Beam system, *IECON Proceedings*, San Jose, CA, USA, 1999, pp. 520–524.
[12] P.H. Eaton, D.V. Prokhorov, D.C. Wunsch II, Neurocontroller Alternatives for "Fuzzy" ball-and-beam systems with nonuniform nonlinear friction, *IEEE Transactions on Neural Network* 11 (2) (2000) 423–435.
[13] X. Fan, N. Zhang, S. Teng, Trajectory planning and tracking of ball and plate system using hierarchical fuzzy control scheme, *Fuzzy Sets and Systems* 144 (2) (2003) 297–312.
[14] J. Lin, J.H. Zhan, Julian. Chang, Stabilization and equilibrium control of new pneumatic cart–seesaw system, *Robotica* 26 (2) (2008) 219–227.
[15] H.P. Lee, Dynamic response of a beam with a moving mass, *Journal of Sound and Vibration* 191 (2) (1996) 289–294.
[16] U. Lee, Separation between the flexible structure and the moving mass sliding on it, *Journal of Sound and Vibration* 209 (5) (1998) 867–877.
[17] S. Park, W.K. Chung, Y. Youm, J.W. Lee, Motion analysis of a moving elastic beam with a moving mass, *Proceedings of the IEEE/ASME International Conference on Advanced Intelligent Mechatronics*, Atlanta, GA, September 19–23, 1999, pp. 167–172.
[18] S. Park, W.K. Chung, Y. Youm, J.W. Lee, Natural frequencies and open-loop responses of an elastic beam fixed on a moving cart and carrying an intermediate lumped mass, *Journal of Sound and Vibration* 230 (3) (2000) 591–615.
[19] S. Park, Y. Youm, Motion of a moving elastic beam carrying a moving mass-analysis and experimental verification, *Journal of Sound and Vibration* 240 (1) (2001) 131–157.
[20] S. Park, B.K. Kim, Y. Youm, Single-mode vibration suppression for a beam–mass–cart system using input preshaping with a robust internal-loop compensator, *Journal of Sound and Vibration* 241 (4) (2001) 693–716.
[21] J. Lin, W.-S. Chao, Vibration suppression control of beam–cart system with piezoelectric transducers by decomposed parallel adaptive neuro-fuzzy control, *Journal of Vibration and Control* doi:10.1177/1077546309104184.
[22] S. Chen, S., Z. Cao, Z., A new method for determining locations of the piezoelectric sensor/actuator for vibration control of intelligent structures, *Journal of Intelligent Material Systems and Structures* 11 (2) (2000) 108–115.
[23] D. Halim, S.O.R. Moheimani, Spatial resonant control of flexible structures—application to a piezoelectric laminated beam, *IEEE Transactions on Control System Technology* 9 (1) (2001) 37–53.
[24] A.J. Fleming, S. Behrens, S.O.R. Moheimani, Optimization and implementation of multimode piezoelectric shunt damping systems, *IEEE/ASME Transactions on Mechatronics* 7 (1) (2002) 87–94.
[25] S.O.R. Moheimani, A.J. Fleming, *Piezoelectric Transducers for Vibration Control and Damping*, Springer, USA, 2006.
[26] B. Samanta, Active control of flexible robot arms using the concept of intelligent structures, *IEEE International Workshop on Intelligent Robots and Systems*, Ibaraki, Japan, 1990, pp. 941–947.
[27] J. Lin, C.C. Lin, H.-S. Lo, Pseudo-inverse Jacobian control with gray relational analysis for robot manipulators mounted on oscillatory bases, *Journal of Sound and Vibration* 326 (3–5) (2009) 421–437.